Electron Transfer Dynamics in Semiconductor–Chromophore–Polyoxometalate Catalyst Photoanodes

‡ Xu Xiang,[a,b] ‡ John Fielden,[a,c] William Rodríguez-Córdoba,[a] Zhuangqun Huang,[a] Naifei Zhang,[a] Zhen Luo,[a] Djamaladdin G. Musaev,[a] Tianquan Lian,*[a] and Craig L. Hill*[a]

[a] Department of Chemistry and Cherry L. Emerson Center for Scientific Computation, Emory University, Atlanta, Georgia 30322, United States

[b] State Key Laboratory of Chemical Resource Engineering, Beijing University of Chemical Technology, Beijing 100029, PR China

[c] WestCHEM, School of Chemistry, University of Glasgow, Glasgow, G12 8QQ, United Kingdom.

ABSTRACT: Triadic photoanodes have been prepared based on nanoporous films of the metal oxides ZrO_2, TiO_2 and SnO_2, sensitizer $[Ru(bpy)_2(dpbpy)]^{2+}$ (P2) and polyoxometalate water oxidation catalyst $[\{Ru_4O_4(OH)_2(H_2O)_4\}(\gamma\text{-}SiW_{10}O_{36})_2]^{10-}$ (**1**), and investigated for their potential utility in water-splitting dye-sensitized photoelectrochemical cells. Transient visible and mid-IR absorption spectroscopic studies were carried out to investigate the charge separation dynamics of these systems, indicating that the electron transfer from photoexcited P2 to TiO_2 and SnO_2 is still the main excited state quenching pathway in the presence of **1**. Furthermore, the accelerated recovery of the P2 ground state bleach in the presence of **1** results from ultrafast (nanosecond) electron transfer from catalyst to oxidized dye. Catalyst loading appears to depend largely on the point of zero charge of the supporting oxide and as such is significantly lower on SnO_2 than on TiO_2: nonetheless, the rate of recovery of the ground state bleach is similar in both TiO_2-P2-**1** and SnO_2-P2-**1** films. Spectral evidence for the formation of long-lived charged separated states is provided by the observation of signals persisting beyond 0.5 μs which are attributed to Stark effect induced change of the P2 spectrum and/or formation of oxidized **1**. Photoelectrochemical measurements on TiO_2-P2 and TiO_2-P2-**1** photoanodes under visible light irradiation indicate a *ca*. 100% photocurrent enhancement in the presence of **1**, suggesting light-driven water oxidation by the TiO_2-P2-**1** system with an internal quantum efficiency of *ca*. 0.2%. The fast formation and long lifetime of the photo-oxidized catalyst suggest that photoanodes of this type may reward further optimization through the introduction of faster catalysts and stabilization of the binding of the dye to the electrode.

Introduction

Efficient water oxidation remains a key challenge in the development of systems for the production of fuel from water. Despite considerable progress in recent years,[1] molecular water oxidation catalysts (WOCs) with the necessary combination of speed and stability have not yet been developed, nor have methods for incorporating them into fuel producing photoelectrochemical devices been optimized.[2] Several water oxidizing photoanodes based on incorporation of water oxidation catalysts into dye-sensitized TiO_2 have been reported,[3] but so far these suffer from low efficiencies and low turnover numbers which have been attributed to the failure of electron transfer from catalyst to dye to compete with recombination from the metal oxide.[3a,d] Successful engineering of such devices will therefore require not only fast, stable catalysts and efficient, stable light absorbers, but rapid, directional electron transfer from the water oxidation catalyst to the oxidized light absorber: so that the desired oxidation of water can outcompete recombination processes.

Recently, a number of fast, oxidatively stable molecular water oxidation catalysts based on polyoxometalates (POMs) have been reported,[4] including $[\{Ru_4O_4(OH)_2(H_2O)_4\}(\gamma\text{-}SiW_{10}O_{36})_2]^{10-}$ (**1**) and $[Co_4(H_2O)_2(PW_9O_{34})_2]^{10-}$. Homogeneous water oxidation using these catalysts can be efficiently driven by light, with $[Ru(bpy)_3]^{2+}$ as photosensitizer and persulfate as oxidant,[5] but turnover numbers in these conditions are limited by degradation of the dye. As electron transfer from catalyst to dye is primarily diffusion controlled in this system,[6] and the dye is most vulnerable to degradation in its oxidized state,[7] it is likely that dye degradation can be mitigated on a photoelectrode where a close contact exists between the two components and transfer of electrons from the catalyst occurs rapidly after oxidation of the dye. Studies of **1** incorporated into TiO_2 photoelectrodes sensitized by $[Ru(bpy)_2(dpbpy)]^{2+}$ (dpbpy = 4,4'-diphosphonic acid-2,2'-bipyridine) and Ru470 have revealed accelerated recovery of the bleach of the dye ground state absorption in the presence of **1**,[6] but have not proven that this is due to the desired electron transfer. Here, we present a comprehensive (fs to μs) photophysical study of triadic photoelectrodes where **1** is supported on the dye-sensitized metal oxides ZrO_2, TiO_2 and SnO_2 (sensitizer = $[Ru(bpy)_2(dpb)]^{2+}$); and provide the first evidence that such POM functionalized electrodes can oxidize water. Variation of acceptor properties and IR detection of injected electrons allows us to confirm ultra-fast catalyst-to-dye electron transfer and generation of the long-lived charge separated states necessary for water oxidation.

Experimental

Materials. TiO_2 and SnO_2. colloids were synthesized following published procedures.[8a-d] ZrO_2 colloids were prepared according to a modified literature procedure[8e] which is detailed below. The photosensitizer $[Ru(bpy)_2(dpb)]Cl_2$ (P2),[9] polyoxometalate water-oxidation catalyst $Rb_8K_2[\{Ru_4O_4(OH)_2(H_2O)_4\}\gamma\text{-}SiW_{10}O_{36})_2]$ (Rb_8K_2[**1**]),[4a] tetraheptylammonium nitrate ([THpA]NO_3),[10] and catalytically inactive polyoxometalate $K_{10}[[Zn_4(H_2O)_2(PW_9O_{34})_2]\bullet 20H_2O$ (K_{10}[**2**])[11] were all synthesized according to published methods. All other chemicals were purchased as analytical grade and used as received.

General Physical Measurements. UV-Vis spectra were acquired using Agilent 8453 spectrophotometer equipped with a diode-array detector and an Agilent 89090A cell temperature controller unit. Spectroelectrochemical measurements were obtained by combining the spectrophotometer with a BASi CV-50W electrochemical workstation. A three-electrode configuration was used in a quartz cell with an FTO supported film as the working electrode, Ag/AgCl reference electrode and Pt counter electrode. The electrolyte was 0.1 M NBu_4PF_6 in acetonitrile, acidified with a drop of concentrated $HClO_4$ (aq). Photoelectrochemical experiments were performed using a 10 mL, 1 cm path length quartz cell and a Hamamatsu Xenon lamp (C2577) filtered to 420 – 470 nm (power after filtering *ca*. 15 mW). TiO_2-P2-**1** films were placed in a cell with the surface perpendicular to the irradiation beam. The illuminated area was ~0.5 cm^2. The potentiostat and electrode configuration was the same as for the spectroelectrochemistry. The buffer/electrolyte was 30 mM $NaSiF_6$ adjusted to pH 5.8 using $NaHCO_3$ (final concentration *ca*. 63 mM).

Film preparation and characterization. Transparent metal oxide films were prepared by spreading their colloidal suspensions onto sapphire windows or FTO conductive glasses by a doctor-blade technique, using one layer of Scotch tape to control the area and thickness. The films were calcined at 400°C for 90 minutes, then sensitized by soaking in an acidic solution of P2 (0.2 mM in 0.1M $HClO_{4(aq)}$) for 24 hours. A further 24 hour soak in 0.1 M $HClO_{4(aq)}$ was used to remove free or weakly-adsorbed dye molecules. The dye-sensitized films were rinsed with water and dried in air. Triadic metal oxide-dye-POM assemblies for ultrafast spectroscopic studies were prepared by soaking the dye-sensitized films in an aqueous solution of Rb_8K_2[**1**] (*ca*. 2 mM) for 30 min, rinsing with water, and drying in air. For photoelectrochemistry, triadic assemblies were instead prepared by soaking TiO_2-P2 films in a toluene solutions of the hydrophobic $THpA_{8.5}H_{1.5}$[**1**] and $THpA_{9.5}Li_{0.5}$[**2**] salts for 5 minutes, rinsing with toluene and air drying. Dye-to-polyoxometalate ratios in several TiO_2-P2-**1** films were estimated by using the extinction coefficient measured for P2 (11700 M^{-1} cm^{-1} at 454 nm) to calculate the loading of dye, and digesting the film using NaOH to allow measurement of the loading of POM by ICP-OES for W (Galbraith Laboratories). The ICP-OES result was used to calibrate UV-vis measurements of the quantity of **1** on other films, by estimating ε = 32000 M^{-1} cm^{-1} at 450 nm for this POM on the dye sensitized metal oxide surfaces.

Synthesis of nanocrystalline ZrO_2 colloids. ZrO_2 particles (38 g, colloidal dispersion 20% in H_2O) were mixed with 3g acetic acid (100%) in a beaker and stirred at room temperature for 36 hr. The uniform solution was poured into an autoclave and kept at 240 °C for 72 hr. The resulting suspension was sonicated for 5 min and transferred into a vial. 3 g of Carbowax 20,000 was added into the suspension and stirred for 24 hr. Finally, the uniform ZrO_2 colloid was obtained for film preparation.

Synthesis of $THpA_{8.5}H_{1.5}[\{Ru_4O_4(OH)_2(H_2O)_4\}(\gamma\text{-}SiW_{10}O_{36})_2]$ ($THpA_{8.5}H_{1.5}$[1]). A solution of $Rb_8K_2[\{Ru_4O_4(OH)_2(H_2O)_4\}(\gamma\text{-}SiW_{10}O_{36})_2]\bullet 25H_2O$ (Rb_8K_2[**1**], 80 mg, 0.012 mmol) in deionized water (8 mL) was added in 2 mL portions to a solution of [THpA]NO_3 (38 mg, 0.079 mmol) in toluene (10 mL). The biphasic mixture was vigorously shaken after each addition of Rb_8K_2[**1**], with the brown aqueous layer initially becoming colorless, but retaining the color after addition of the later portions. Two drops of aqueous 1 M HCl were then added and the mixture shaken for a further 2 minutes. The organic layer was separated and dried, the solvent removed *in vacuo*, then redissolved in dichloromethane allowing $THpA_{8.5}H_{1.5}$[**1**] (80 mg, 0.0089 mmol, 75% based on POM) to be recovered by evaporation as a dark brown powder. FTIR (diamond anvil) cm^{-1}: 3430 w, 2955 s, 2923 s, 2855 s, 1709 w, 1630 w, 1483 m, 1466 m, 1378 m, 1341 m, 1260 s, 1086 s, 1017 s, 956 s, 880 s, 793 vs, 751 vs, 721 vs, 543 m. UV-vis (CH_3CN) nm (L mol^{-1} cm^{-1}): 267 (shoulder, 65900), 451 (24000). Elemental analysis for $C_{238}H_{521.5}N_{8.5}O_{82}Ru_4Si_2W_{20}$ ($THpA_{8.5}H_{1.5}$[**1**]) calcd (found) %: C 31.93 (32.20), H 5.87 (6.03), N 1.33 (1.47). TGA shows no mass loss from 25 to 200 °C, and 39% mass loss between 200 and 450 °C (calcd 39.8%).

Synthesis of $THpA_{9.5}Li_{0.5}[Zn_4(H_2O)_2(PW_9O_{34})_2]\bullet 3H_2O$ ($THpA_{9.5}Li_{0.5}$[2]). $K_{10}[Zn_4(H_2O)_2(PW_9O_{34})_2]\bullet 20H_2O$ (100 mg, 0.018 mmol) was dissolved in deionized water (5 mL) by heating, and 1 mL of aqueous 1 M LiCl was added. The resulting solution was added in 2 mL portions to a solution of [THpA]NO_3 (75 mg, 0.016 mmol) in toluene (10 mL). The biphasic mixture was vigorously shaken after each addition of the $K_{10}[Zn_4(H_2O)_2(PW_9O_{34})_2]\bullet 20H_2O$ solution. Another 1 mL of LiCl solution was added and the layers allowed to separate overnight. The organic layer was evaporated to dryness *in vacuo*, and the resulting waxy solid extracted by trituration with diethyl ether until it became a white crystalline solid ([THpA]NO_3). After filtration, the diethyl ether washings were evaporated to dryness yielding **$THpA_{9.5}Li_{0.5}$[2]** (83 mg, 0.0095 mmol, 53% based on POM) as an off-white waxy solid. FTIR (diamond anvil) cm^{-1}: 3430 w, 2954 s, 2924 vs, 2855 s, 1630 w, 1481 w, 1466 m, 1377 m, 1338 m, 1261 m, 1079 m, 1033 s, 937 s, 885 m, 777 vs, 723 vs, 589 w. UV-vis (CH_3CN) nm (L mol^{-1} cm^{-1}): 258 (58900). Elemental analysis for $C_{266}H_{580}Li_{0.5}N_{9.5}O_{73}P_2W_{18}$ calcd (found) %: C 36.65 (36.36), H 6.71 (6.52), N 1.53 (1.57). TGA shows a 1.3% mass loss between 25 and 200 °C (calcd 0.4% for 3 uncoordinated H_2O) and a further 43.3 % between 200 and 450 °C (calcd 45.2 % for 9.5 THpA and 2 coordinated H_2O).

Ultrafast Visible Transient Absorption Measurements. The femtosecond transient absorption spectrometer is based on a regeneratively amplified Ti:sapphire laser system (coherent Legend, 800 nm, 150 fs, 3 mJ/pulse and 1 kHz repetition rate) and a Helios spectrometer (Ultrafast Systems LLC). The excitation pulse at 400 nm was generated by doubling the frequency of the fundamental 800 nm pulse using a β-barium borate (BBO) type I crystal. The energy of the 400 nm pump pulse was set to ~250 nJ/pulse with a neutral density filter. The pump beam diameter at the sample was ~400 μm, corresponding to an excitation density of ~2 μJ/cm^2 per pulse. A white light continuum (WLC) (450~720 nm), used as a probe, was generated by attenuating and focusing 10 μJ of the fundamental 800 nm pulse into a sapphire window. This WLC

was split in two parts used as a probe and reference beams. The probe beam was focused with an aluminum parabolic reflector into the sample with a beam diameter of ~150 μm. The reference and probe beams were focused into a fiber-coupled multichannel spectrometer with CMOS sensors and detected at a frequency of 1 kHz. To minimize low-frequency laser fluctuations every other pump pulse was blocked with a synchronized chopper (New Focus Model 3501) at 500 Hz, and the absorbance change was calculated with two adjacent probe pulses (pump-blocked and pump-unblocked). The delay between the pump and probe pulses was controlled by a motorized translational stage. Samples were mounted on a stage and constantly moved by a controller throughout the measurements to avoid the destruction of samples. In all transient absorption spectra, the chirp and time zero correction were performed with Surface Explorer software (v.1.1.5, Ultrafast Systems LCC). The typical instrument response of our spectrometer is well represented by a Gaussian function with a full width at half-maximum (FWHM) of 180 ± 10 fs.

Nanosecond Transient Absorption Measurements. Measurements at the ns to μs timescales were carried out in an EOS spectrometer (Ultrafast Systems LLC). The pump pulses at 400 nm were generated from the same laser system described above. The probe pulse, a 0.5 ns white-light source operating at 20 kHz, was synchronized with the femtosecond amplifier, and the delay time was controlled by a digital delay generator. The probe light was detected in a fiber-optic-coupled multichannel spectrometer with a complementary metal−oxide−semiconductor (CMOS) sensor. The absorbance change was calculated from the intensities of sequential probe pulses with and without the pump.

Ultrafast Visible Pump/IR Probe Transient Absorption Measurements. Our tunable femtosecond infrared spectrometer is based on a Clark IR optical parametric amplifier (OPA) which generates two tunable near-IR pulses in the 1.1 to 2.5 μm spectral range (signal and idler, respectively). The broad mid-IR pulses centered at 2000 cm^{-1} were generated by difference frequency generation (DFG) combining the corresponding signal and idler in a 1-mm-thick type II $AgGaS_2$ crystal. Frequency tuning of the mid-IR pulses was achieved by changing the signal and idler frequencies at the OPA and optimizing the timing between the pulses and the phase matching angles of the BBO (OPA crystal) and the $AgGaS_2$ crystal. After difference frequency generation, the mid-IR pulse was collimated and split in two parts with a 90% beam splitter. The 10% transmitted part was used as a probe in the visible pump-IR probe transient absorption measurements. To prevent cumulative heating in the sample and to avoid the saturation of the detector, the intensity of the probe mid-IR pulse was attenuated using neutral density filters to approximately 40 μJ, before it was focused into a 0.4 μm CaF_2 path-length cell containing the sample. At the focal point, the probe was spatially overlapped with the temporally delayed 400 nm with a pump beam with energy of about 2 μJ per pulse. To avoid rotational diffusion effects, the polarization angle of the excitation beams were controlled with a half-wave plate and set to the magic angle (54.7°) relative to the probe beam. The diameter of the pump and probe beams were 400 and 200 μm, respectively. The mid-infrared probe pulse was spectrally dispersed with an imaging spectrograph (CVI, Digikrom 240) and imaged onto a 32-element infrared HgCdTe (MCT) array detector. The difference absorption spectra were calculated by subtracting the absorption spectrum of the excited sample from the absorption spectrum of the sample in the ground state by blocking every other pump pulse with a phase-locked optical chopper (New Focus) at 500 Hz. The instrument response function of our spectrometer was well represented by a Gaussian function with a 230 ± 10 full width at half-maximum (FWHM) for the VIS-IR setup.

Results and Discussion

Film Assembly and Characterization. The metal oxide films were sensitized with P2 in acidic conditions, according to published methods.[12] For photoelectrochemical measurements, TiO_2-P2 films were treated with toluene solutions of the hydrophobic $THpA_{8.5}H_{1.5}$[**1**] salt, as deposition of $THpA^+$ cations at the electrode surface helps stabilize the binding of **1** in aqueous buffers. For ultrafast spectroscopic studies, the sensitized ZrO_2, TiO_2 and SnO_2 aqueous solutions of Rb_8K_2[**1**] were used as they provided better transparency.

Although the impact of P2 on the film's overall surface charge is unclear, due to its dependence on the level of protonation of the phosphonate binders *vs* the displaced ligands (P2 can have overall charges from -2 to +2 depending on protonation state), it is clear that the negatively charged (10-) **1** binds to the film surface through electrostatic interactions. In aprotic solvents (e.g. toluene) any available protons will be bound by the film, and the aqueous solution used to apply **1** has a pH of 3, well below the point-of-zero charge (pzc) of all three oxides. There should also be a strong *local* electrostatic interaction between the dye Ru^{2+} centers and **1**: despite the apparent absence of static quenching interactions between $[Ru(bpy)_3]^{2+}$ in a previous solution based study,[6a] the aqueous high ionic strength conditions used do not pertain to the film. The quantities of P2 and **1** have been estimated using UV-vis spectroscopy on the assembled films (see Figures S1 to S3 in the SI), combined with ICP-OES for W on base digested films to confirm the quantity of POM (the extinction coefficient of **1** varies according to its protonation state).[4c] For films assembled using aqueous **1**, this furnished P2:**1** ratios of 8:1 (ZrO_2), 11:1 (TiO_2) and 19:1 (SnO_2), qualitatively agreeing with the trend in pzc which falls from around pH 6.5 for ZrO_2, to pH 6 for TiO_2 and pH 4.5 for SnO_2.[13] Thus, SnO_2 carries the least positive surface charge and ZrO_2 the most positive, and the charge introduced by the dye appears to have less influence on the loading of **1** than the intrinsic properties of the metal oxide surface. A similar trend is observed in the absorption of **1** onto bare metal oxide films (Figures S4, S5 in the SI). The TiO_2-P2 films treated with $THpA_{8.5}H_{1.5}$[**1**] in toluene have an estimated P2:**1** ratio of 8:1, rather higher than that seen for aqueous deposition. This is probably because interactions between **1** and the positively charged electrode surface are stronger in the less polar toluene solvent.

Infra-red Transient Spectroscopy. Electron injection from various photosensitizers to semiconducting metal oxides has been extensively studied,[14] but there are fewer reports on the photophysical behavior of related systems incorporating water oxidation catalysts.[3a,d-h,6] Dye sensitized TiO_2 films treated with **1** have previously been studied by transient visible spectroscopy,[6a] demonstrating accelerated recovery of the oxidized dye in the presence of catalyst. However, transient visible measurements alone cannot confirm whether this accelerated recovery is due to the desired catalyst-to-sensitizer electron transfer, or if quenching of the dye by the catalyst and/or accelerated recombination from the metal oxide play a role.

Energy levels of the metal oxides ZrO_2, TiO_2 and SnO_2, the P2 photosensitizer and water oxidation catalyst **1** are summarized in Scheme 1: as well as the $(Ru^{IV})_4$ HOMO energy level, which is thermodynamically capable of transferring electrons to the hole in the P2 HOMO, the POM also has a $(Ru^{IV})_3Ru^{III}$ LUMO which is a more thermodynamically favorable acceptor than the TiO_2 conduction band. Energy transfer from P2 to **1** is also possible, as the latter shows appreciable absorbance up to 700 nm (Figures S6 in the SI).

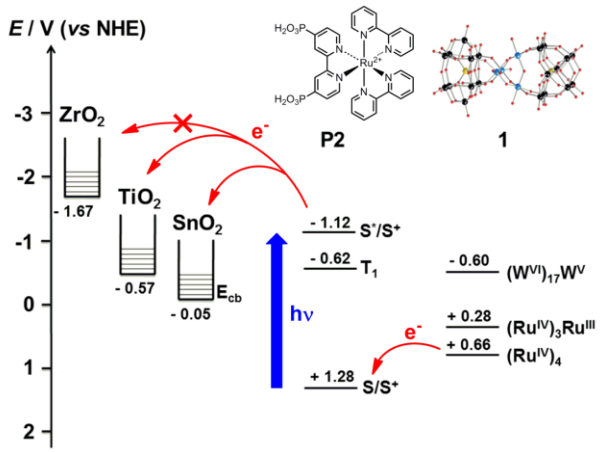

Scheme 1 Simplified energy levels and proposed electron transfer processes in the MO_2-P2-1 triads. The energy levels of 1 and $E(S/S^+)$ of P2 are electrochemically determined values found in the literature.[4c,14h] $E(S^*/S^+)$ was calculated based on the pump energy. $E(T_1)$ was obtained from its emission spectroscopy (Figure S7, SI). For clarity, several closely spaced POM energy levels immediately above the $(Ru^{IV})_3Ru^{III}$ LUMO and below the $(Ru^{IV})_4$ HOMO are omitted.

The conduction band position for TiO_2 is around 0.5 V (at pH 7) higher than that of SnO_2, while ~ 1V lower than that of ZrO_2 (see Scheme 1).[14f,g, 18] Therefore, electron injection from excited-state P2 into ZrO_2, TiO_2 and SnO_2 films has been investigated by time-resolved mid-IR transient absorption measurements (pump 515 nm, probe 5000 nm) in the absence or presence of **1** (Figure 1), along with measurements of POM treated metal oxides in the absence of P2. Note that the samples were pumped at 515 nm to minimize the excitation of the metal oxide films themselves. Unsurprisingly, the dye free control measurements (Figures S8 and S9 in the SI) indicate no electron injection: although **1** has a large visible extinction coefficient,[4c] the nature of the process giving rise to the absorption is unclear and the excited state is short lived (< 20 ps).[15] It is therefore likely that electronic coupling between the metal oxides and the POM is not strong enough for electron transfer to compete with the rapid excited state decay.

Measurements on the dye-sensitized oxides indicate that electron injection occurs on TiO_2 and SnO_2 in the presence and absence of **1** (Figure 1), and confirm that the conduction band edge potential of ZrO_2 is too negative to allow electron injection from the excited states of P2 (Figure S10, SI). For TiO_2, the kinetics of electron injection from P2 are biphasic, consisting of an ultrafast ~0.3 ±0.1 ps component and a slower component that can be fitted by multi-exponential rise with time constants of several to hundreds of picoseconds. Respectively, these correspond to injection from the unrelaxed ^{1}MLCT and relaxed ^{3}MLCT excited states of the dye.[8d] Similar biphasic electron injection kinetics from related ruthenium polypyridyl dyes to TiO_2 has been reported by many groups.[8e,16] For TiO_2-P2-**1** there is still a fast electron injection within ~0.3 ps, similar to that of sensitized TiO_2. However, the kinetics and amplitude of the slow injection component are altered. In addition, there is a small decay process (~10%) extending beyond ~600 ps (detection limit). The origin of this decay is not clear, but it likely results from the relaxation of the injected electrons in TiO_2[16a]. Similar relaxation likely also exists in TiO_2-P2, but the overall IR absorption signal increases due to the presence of the slow injection component. There are two likely reasons for the reduction of the slow injection component in the TiO_2-P2-**1** triad. Firstly, because the ^{3}MLCT is close to the conduction band edge of TiO_2, the injection rate is sensitive to the conduction band edge position, which may be affected by the presence of the highly negatively charged POM. Secondly, the presence of lower lying vacant orbitals on **1** may provide a more thermodynamically favorable electron acceptor for the excited P2. However, it should be emphasized that the initial amplitude of the IR signal (and hence number of electrons injected) varies only slightly in the presence of **1**, suggesting that electron transfer from excited P2 to TiO_2 is still the main quenching pathway in the triad.

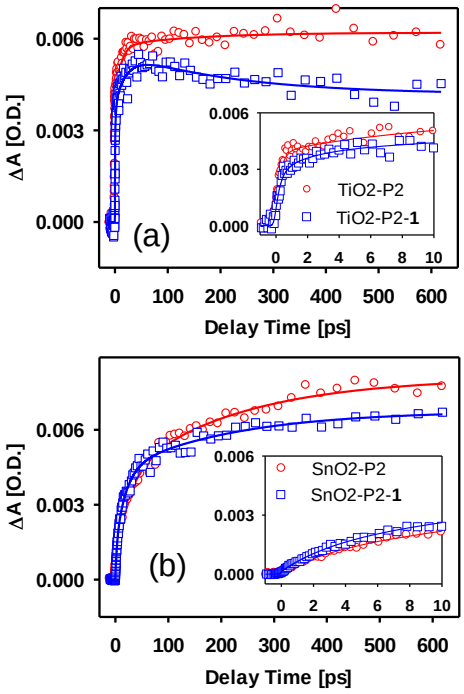

Figure 1. Electron injection kinetics measured by mid-IR transient absorption spectroscopy (excitation 515 nm, 5000 nm probe): (a) TiO_2-P2 (red circles) and TiO_2-P2-1 (blue squares); (b) SnO_2-P2 (red circles) and SnO_2-P2-1 (blue squares).

In the case of SnO_2-P2, only 50% of the electrons (referenced to the signal at 600 ps) are injected within the first 30 ps (Figure 1b), and the signal continues to slowly increase up until the detection limit of 600 ps. The lack of ultrafast injection component (~0.3 ps) is consistent with the injection kinetics of other Ru-bipyridyl complexes on SnO_2.[17a] These kinetics are different from those of P2 on TiO_2, and can be attributed to the much lower density of states in SnO_2, in which electron injection from the ^{1}MLCT state cannot compete effectively with the ultrafast intersystem crossing to the ^{3}MLCT

state,[14a,17] even though the conduction band edge of SnO_2 is lower in energy (-0.05 V compared to -0.57 V vs NHE at pH 7).[18] As a result, the slow injection from the ^{3}MLCT state dominates the injection kinetics. Similarly to TiO_2-P2-**1** vs TiO_2-P2, a slight decrease of the slow injection component is also observed in the SnO_2-P2-**1** compared to SnO_2-P2, which can also be attributed to the likely alteration of the injection kinetics to SnO_2 as well as the possible P2 to **1** charge transfer process. It should be noted that while *faster* recombination is cited as a reason for the poorer performance of SnO_2 based DSSCs,[19] this process occurs between the metal oxide surface and I_3^-, which is absent in our work.

Transient Visible Spectroscopy. Transient visible absorption measurements were performed on the various MO_2-P2 (M=Zr, Ti and Sn) films, on fs to μs timescales with 400 nm excitation (Figure 2). In the case of ZrO_2-P2 and ZrO_2-P2-**1**, it is known that no electron injection to the metal oxide occurs, so that the spectral features observed represent the difference between the ground and excited states of P2. A strong ground state bleach (GSB) is observed centered at 455 nm, and a broad positive excited state absorption is observed at $\lambda > 530$ nm, the decay kinetics of which are consistent with each other, indicating that the observed decay can be attributed to regeneration of the P2 ground state from the excited state. The decay can be fitted by a multi-exponential function from which we obtain a half-life time of the excited state of 102 ps (Figure 3). This lifetime is significantly shorter than that for P2 in solution (Figure S11 in the SI). The shortened lifetime is likely due to self-quenching between excited P2 molecules on the film.[14a] Transient absorption spectra in the presence of **1** are similar to those without POM, although the GSB decay is slightly faster (with a half-life time of 42 ps). This may indicate some quenching of the P2 excited state by **1**, as observed in solution (Figure S12, SI). On the basis of the current data it is not possible to say whether this quenching occurs by electron or by energy transfer, although in solutions of $Ru(bpy)_3^{2+}$ and **1** it has recently been ascribed to rapid electron transfer to the catalyst followed by recombination.[20] Importantly though for interpretation of the results on TiO_2 and SnO_2, electron injection to oxide is the main (and much faster) excited state decay channel (see below) and the effect of excited state quenching by **1** is minor in comparison.

For TiO_2-P2 electrons are rapidly injected into the metal oxide conduction band, so the amplitude of the ground state bleach observed at around 455 nm in this case largely reflects the amount of oxidized P2. Correspondingly, the transient absorption spectra of the sensitized TiO_2 film show distinct features from those of the sensitized ZrO_2 film (Figure S13) at $\lambda > 530$ nm where excited/oxidized state absorptions are observed. The decay of the GSB is also significantly slower than on ZrO_2 (a half-life time of *ca*. 6.9 ns, Figure 3b). In this case, decay of the GSB results from recombination of electrons injected into TiO_2 with the oxidized dye moieties, and the process is still not complete at 1 μs. Addition of **1** to TiO_2-P2 significantly speeds the recovery of the P2 GSB. The absorbance is around 70% recovered within 1 ns, and complete recovery occurs inside around 10 ns (half life *ca*. 127 ps). This is in marked contrast to previous ns flash photolysis measurements on this system, which suggested recovery might still not be complete after several microseconds.[6a]

From transient IR measurements and measurements on ZrO_2-P2-**1**, we know that (i) the total yield of injected electrons to TiO_2 and SnO_2 is similar in both presence and absence of **1**, (ii) charge recombination is at most slightly enhanced by the presence of **1** and (iii) direct quenching of excited P2 by **1** is not a significant process compared to electron injection into the metal oxide. Therefore, the rapid regeneration (*ca*. 1 ns) of P2 in the triads must be due to electron transfer from **1** to the oxidized dye, generating the kind of charge separated state required for water oxidation. The timescale for this regeneration is much faster than observed for **1** and $[Ru(bpy)_3]^{2+}$ in solution (*ca* 20 μs with a 1:1 dye:POM ratio), or for comparable sensitized electrodes where dyes are covalently connected to IrO_2 nanoparticles (2.2 ms),[3a] and is also significantly faster than typical for regeneration of Ru-polypyridyl dyes by I^- in DSSCs.[21] As dye degradation is largely believed to occur in the Ru^{3+} state, this ultrafast electron transfer is potentially very positive for the prospects of creating stable devices based on Ru-polypyridyl dyes and POM water oxidation catalysts.

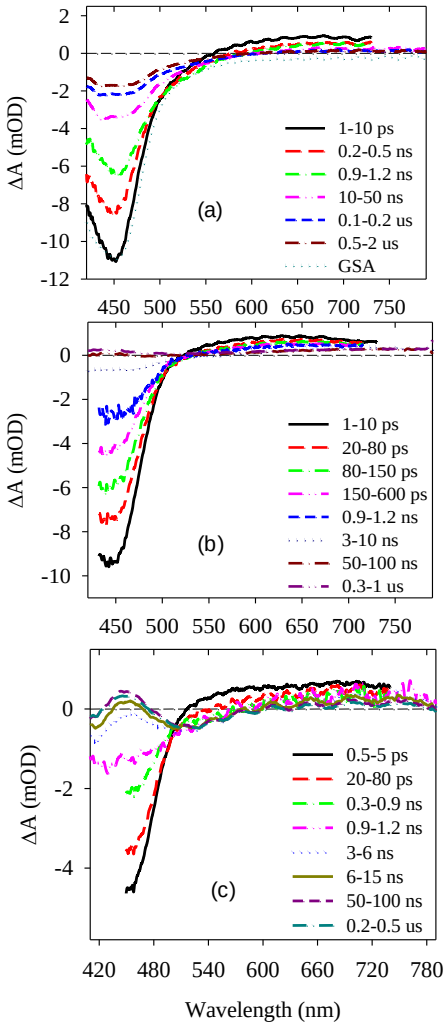

Figure 2. Transient differential absorption spectra of (a) TiO_2-P2, (b) TiO_2-P2-**1** and (c) SnO_2-P2-**1** at indicated delay time windows after 400 nm excitation. Also shown in (a) is the steady state absorption spectrum of P2 (green dotted line, GSA), which has been inverted for better comparison with the bleach.

SnO_2-P2 shows a slower GSB recovery than TiO_2-P2 (a half-life time *ca.* 1.1 μs, Figure 3c). It is also interesting to note the slight growth of the P2 bleach on the < 600 ps time scale, which likely reflects the slow injection process in this

system seen in our infrared measurements. The absorptions of the oxidized state overlap less with the GSB than do those of the excited state, leading to the observed slow increase in the intensity of the bleach as P2 evolves from the excited to the oxidized state. Just as on TiO_2, the presence of **1** speeds the GSB recovery: in this case quite dramatically. The ground state absorption is 65% recovered after 1 ns and recovery is complete at around 10 ns (half life *ca*. 520 ps), giving a very similar overall result to the TiO_2-P2-**1** triad. The similarity of the bleach recovery rates on the two oxides in the presence of catalyst, despite inherently different recombination rates in the dyads, provides further evidence that bleach recovery must primarily be due to electron transfer from the catalyst to oxidized P2.

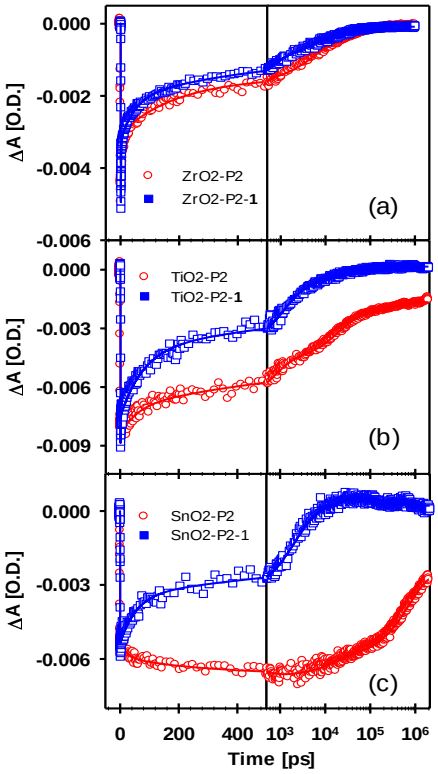

Figure 3. Excited/charge separated state decay kinetics for MO_2-P2 and MO_2-P2-**1** averaged over 460-470 nm (400 nm excitation). The time axis is linear for the left panel and logarithmic scale for the right panel.

Both TiO_2-P2-**1** and SnO_2-P2-**1** show a derivative like feature at around 400-600 nm at longer time delays (Figure 2). In the case of SnO_2-P2-**1**, this signal appears earlier (after ~ 2 ns) and is stronger. There are two possible origins for this signal: Stark effect induced change of the P2 spectrum and the change of absorption of **1** in the charge separated state. It has been shown in recent studies of nanoporous oxide films sensitized by Ru bipyridyl complexes similar to P2, that charge injection from the sensitizer to TiO_2 and SnO_2 leads to changes in the sensitizer absorption spectrum that extend beyond the excited molecule and can be well described by the Stark effect caused by the electric field of the injected electron in the oxide.[22] The observed signal in our triad is similar to the derivative shape observed in the dyad and triad reported in the previous paper. However, the derivative like Stark effect signal is not seen in the TA spectra of the TiO_2-P2 and SnO_2-P2 dyads (Figure 2a), which may be attributable to the much larger TA features of the oxidized P2.

In addition to the Stark effect, the formation of an $MO_2(e^-)$-P2-**1**$^+$ charge separated state may also lead to noticeable change in the absorption of **1**. To test whether this positive signal could result from formation of oxidized **1,** spectroelectrochemical measurements were performed on an SnO_2-P2-**1** film supported on FTO. Applying biases of + 500 then + 800 mV (vs Ag/AgCl) indeed resulted in an increase in absorbance at around 450 nm, indicating that the positive signals may also contain contributions from the formation of oxidized **1** (Figure 4). We compared the UV-vis differential spectrum from spectroelectrochemical measurements with the characteristic spectra of transient absorption of SnO_2-P2-**1** (see Figure S14 in the SI). They do not match perfectly, which may indicate that both the Stark effect and the formation of oxidized **1** contribute to the positive signal or that solvent environments have an important influence on this system. Further interpretation is challenging as the visible absorption of **1** varies considerably with both protonation and oxidation state in solution, and establishing the precise behavior of such a species on a metal oxide film is beyond the scope of this study. For reasons yet to be understood, the Stark effect/oxidized 1 feature is much larger in SnO_2-P2-**1** than TiO_2-P2-**1**. It may indicate a larger yield of charge separated state. Furthermore, the SnO_2 film could give rise to a stronger signal from oxidized **1**, despite its lower loading. The lower pzc of SnO_2 means that **1** is more likely to be protonated, which should result in a higher extinction coefficient.[4c]

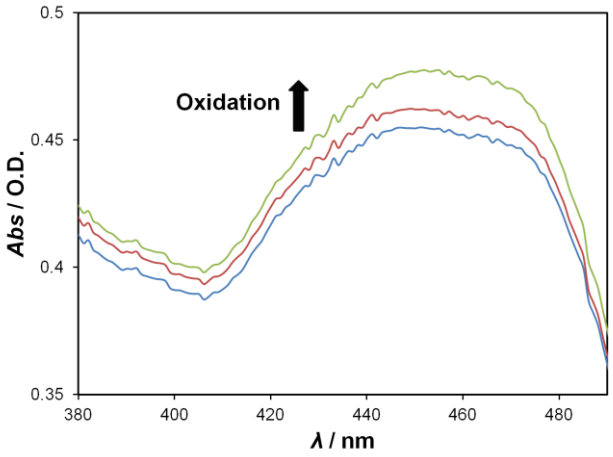

Figure 4. Spectroelectrochemistry of an SnO_2-P2-**1** film with acidified 0.1 M NBu_4PF_6 in acetonitrile as electrolyte. Blue, 0 mV bias; brown, 500 mV bias; green 800 mV bias (*vs*. Ag/AgCl); spectra measured after the film was biased for 5 minutes.

Photoelectrochemical Studies. Figure 5 shows photoelectrochemical (chronoamperometric) measurements on TiO_2-P2, TiO_2-P2-**1** and TiO_2-P2-**2** films at pH 5.8 (**2** is the catalytically inactive POM, $[Zn_4(H_2O)_2(PW_9O_{34})_2]^{10-}$). Upon illumination, all three films show an initial spike resulting from electron injection from P2 into the TiO_2 film – this current then decreases, approaching a steady state. Upon blocking the beam a current spike is observed in the opposite direction, which results from recombination of injected electrons with oxidized P2. The injection and recombination spikes are smaller in the presence of both **1** and **2**, but the pseudo-steady state photocurrent in the presence of WOC **1** is significantly

larger (by about 100%) than for either TiO_2-P2 or TiO_2-P2-**2**. If water is eliminated by using an acetonitrile solution with electrolyte, the photocurrents observed are much smaller and **1** produces no significant increases in photocurrent (see Figure S15, SI). These measurements suggest that the TiO_2-P2-**1** photoanode may be oxidizing water.

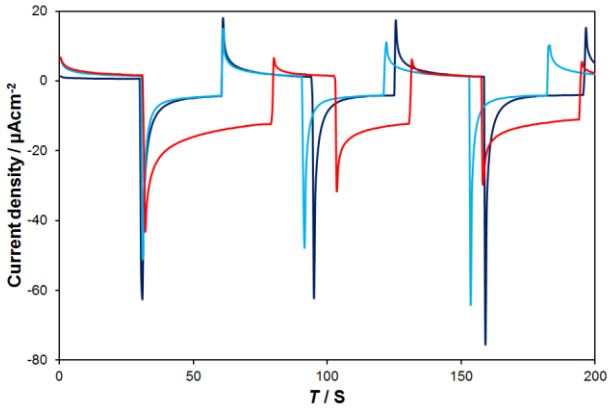

Figure 5 Photoelectrochemical measurements (chronoamperometry) of TiO2-P2 (dark blue), TiO2-P2-**2** (light blue) and TiO2-P2-**1** films (red), at an applied bias of 0 mV vs Ag/AgCl, pH 5.8. Illumination (420 – 470 nm, 30 mW cm^{-2}) was provided by a filtered Xenon lamp.

As in other studies,[3b,c,e] a small pseudo-steady state photocurrent is observed from the sensitizer dye in the absence of catalyst. This photocurrent, indicating continued flow of electrons into TiO_2 after the initial injection, suggests an oxidative process occurs at the photoanode in the absence of catalyst and remains unexplained. Possibilities include oxidation of impurities present in the electrolyte, a low level of water oxidation or destructive oxidation of the sensitizer, and current evidence is inconclusive. The observation of similar effects in several independent studies suggests that impurities in inorganic buffers/electrolytes are not likely to be the explanation. In our case, we note that the photocurrent is substantially smaller when the electrode is immersed in an acetonitrile based, rather than aqueous electrolyte, implying involvement of water. However, photoanodes functionalized solely with P2 do not produce oxygen,[3b] suggesting water oxidation is not the cause. An oxidative degradation of the sensitizer involving reaction with water would therefore seem a likely explanation, although a recent study on the stability of dye-sensitized electrodes found that illumination of TiO_2-P2 electrodes in aqueous media encourages more rapid *desorption* rather than degradation of dye.[23]

Based on the observed steady state photocurrents of *ca.* 15 μAcm^{-2} and the film absorbance of 1.5 a.u., an internal quantum efficiency of *ca.* 0.2% can be estimated for the **1** treated photoanodes in these unoptimized conditions. However, the photoanodes are unstable: in the course of a 20 minute photoelectrochemical experiment approximately 40% of the absorbance at 450 nm is lost. This is primarily due to rapid desorption of P2 in aqueous buffers rather than photo-damage, as soaking the electrode in buffer *without irradiation or bias* results in a comparable loss of absorbance. Higher pH buffers (e.g. phosphate), which are more suitable for efficient operation of the catalyst,[4,5] only worsen the desorption, although the electrodes are reasonably stable in water and unbuffered electrolytes. The rather low quantum efficiency compared to similar systems based on IrO_2 nanoparticles[2a, 3a,d] may be explained by the low loading of catalyst and its relatively low maximum TOF (*ca.* 0.25 s^{-1})[4c] *vs* IrO_2 (*ca.* 40 s^{-1} per surface Ir), which is compounded by the current use of a sub-optimal pH for its operation. Additionally, the measured charge transfer process in our current TAS experiments corresponds only to the first of the four catalyst oxidation events needed for the oxidation of water, and later oxidations are likely to be slower. For these reasons, ongoing studies aim to probe how the catalyst oxidation rate depends on its oxidation state, increase catalyst loading, stabilize sensitizer binding at pH ~ 7 and quantify O_2 from these improved photoelectrodes.

Summary and Conclusions

Photoelectrodes composed of SnO_2 and TiO_2, the dye $[Ru(bpy)_2(dpbpy)]^{2+}$ (P2) and water oxidation catalyst $[\{Ru_4O_4(OH)_2(H_2O)_4\}(\gamma\text{-}SiW_{10}O_{36})_2]^{10-}$ (**1**) rapidly form long-lived charge separated states upon visible light illumination, in which electrons are injected into the metal oxide conduction band and holes are located on the water oxidation catalyst. Formation of these charge separated states appears to be efficient, as there is minimal evidence for competing processes, and is a result of ultrafast (ns) electron transfer from $[\{Ru_4O_4(OH)_2(H_2O)_4\}(\gamma\text{-}SiW_{10}O_{36})_2]^{10-}$ to $[Ru(bpy)_2(dpb)]^{3+}$. Such rapid catalyst-to-dye electron transfer is unusual and potentially very positive for the construction of stable devices based on Ru-polypyridyl dyes and polyoxometalate water oxidation catalysts. Photoelectrochemical measurements show significant (>100%) enhancement of visible light induced photocurrents compared to catalyst-free TiO_2-P2 electrodes, suggesting light driven water oxidation. However, significant improvement in their quantum efficiency (*ca.* 0.2%) and hydrolytic stability is needed for the practical application of these electrodes. One limit on the performance of the current photoelectrodes arises from the relatively low speed of the catalyst in the conditions used (pH 5.8). In addition, water oxidation requires four sequential oxidations of the catalyst and electron transfer rates from these higher oxidation states are currently unknown. Ongoing studies are focused both on probing these later oxidation events, and stabilizing the binding of the sensitizer under buffer conditions more ideally suited to **1** and other, faster, polyoxometalate water oxidation catalysts.

ASSOCIATED CONTENT

UV-visible absorption spectra of the films, additional PEC and transient absorption measurements, and absorption/emission spectra of P2 solutions in the presence and absence of **1** can all be found in the supporting information. This material is available free of charge via the Internet at http://pubs.acs.org.

AUTHOR INFORMATION

Corresponding Authors

* T. Lian, tlian@emory.edu; * C. L. Hill, chill@emory.edu

Author Contributions

The manuscript was written through contributions of all authors. All authors have given approval to the final version of the manuscript. ‡These authors contributed equally.

Notes

The authors declare no competing financial interest.

ACKNOWLEDGMENTS

We acknowledge Dr. Yurii V. Geletii for helpful discussions, and Dr. Jie Song for help with the synthesis of P2. This work was funded by the U.S. Department of Energy, Office of Basic Energy Sciences, Solar Photochemistry Program (DE-FG02-07ER-15906) to CLH, TL and DGM, and by the EU through award of an IOF to JF (POMHYDCAT, contract no. 254339). XX thanks the China Scholarship Council for financial support.

ABBREVIATIONS

MO_2, metal oxides (TiO_2, SnO_2, ZrO_2); P2, $[Ru(bpy)_2(dpb)]^{2+}$; POM, polyoxometalate; $E(S/S^+)$, ground state oxidation potential of P2; $E(S^*/S^+)$, excited state oxidation potential of P2; E(T1), excited state oxidation potential of the thermally equilibrated triplet state of P2; HOMO, highest occupied molecular orbital; LUMO, lowest unoccupied molecular orbital; GSB, ground state bleach; UV-vis, ultraviolet-visible; PEC, photoelectrochemistry.

REFERENCES

(1) (a) Binstead, R. A.; Chronister, C. W.; Ni, J.; Hartshorn, C. M.; Meyer, T. J. *J. Am. Chem. Soc*. **2000**, *122*, 8464. (b) Yagi, M.; Kaneko, M. *Chem. Rev.* **2001**, *101*, 21. (c) Hurst, J. K. *Coord. Chem. Rev*. **2005**, *249*, 313. (d) Zong, R.; Thummel, R. *J. Am. Chem. Soc.* **2005**, *127*, 12802. (e) Eisenberg, R.; Gray, H. B. *Inorg. Chem.* **2008**, *47*, 1697. (f) McDaniel, N. D.; Coughlin, F. J.; Tinker, L. L.; Bernhard, S. *J. Am. Chem. Soc.* **2008**, *130*, 210. (g) Brimblecombe, R.; Swiegers, G. F.; Dismukes, G. C.; Spiccia, L. *Angew. Chem., Int. Ed.* **2008**, *47*, 7335. (h) Concepcion, J. J.; Jurss, J. W.; Brennaman, M. K.; Hoertz, P. G.; Patrocinio, A. O. T.; Iha, N. Y. M.; Templeton, J. L.; Meyer, T. J. *Acc. Chem. Res.* **2009**, *42*, 1954. (i) Hurst, J. K.; Cape, J. L.; Clark, A. E.; Das, S.; Qin, C. *Inorg. Chem.* **2008**, *47*, 1753. (j) Betley, T. A.; Surendranath, Y.; Childress, M. V.; Alliger, G. E.; Fu, R.; Cummins, C. C.; Nocera, *D. G. Philos. Trans. R. Soc., B* **2008**, *363*, 1293. (k) Muckerman, J. T.; Polyansky, D. E.; Wada, T.; Tanaka, K.; Fujita, E. *Inorg. Chem.* **2008**, *47*, 1787. (l) Sala, X.; Romero, I.; Rodríguez, M.; Escriche, L.; Llobet, A. *Angew. Chem., Int. Ed*. **2009**, *48*, 2842. (m) Nakamura, R.; Frei, H. *J. Am. Chem. Soc.* **2006**, *128*, 10668. (n) Jiao, F.; Frei, H. *Angew. Chem., Int. Ed.* **2009**, *48*, 1841. (o) Hull, J. F.; Balcells, D.; Blakemore, J. D.; Incarvito, C. D.; Eisenstein, O.; Brudvig, G. W.; Crabtree, R. H. *J. Am. Chem. Soc.* **2009**, *131*, 8730. (p) Duan, L.; Xu, Y.; Gorlov, M.; Tong, L.; Andersson, S.; Sun, L. *Chem. Eur. J.* **2010**, *16*, 4659. (q) Masaoka, S.; Sakai, K. *Chem. Lett.* **2009**, *38*, 182. (r) Duan, L.; Bozoglian, F.; Mandal, S.; Stewart, B.; Privalov, T.; Llobet, A.; Sun, L. *Nature Chem.* **2012**, *4*, 418.

(2) (a) Youngblood, W. J.; Lee, S.-H. A.; Maeda K.; Mallouk, T. E. *Acc. Chem. Res.*, **2009**, *42*, 1966. (b) Duan, L.; Tong, L.; Xu, Y.; Sun, L. *Energy Environ. Sci.*, **2011**, *4*, 3296. (c) Song, W.; Chen, Z.; Glasson, C. R. K.; Hanson, K.; Luo, H.; Norris, M. R.; Ashford, D. L.; Concepcion, J. J.; Brennaman, M. K.; Meyer, T. J. *Chem. Phys. Chem.* **2012**, *13*, 2882.

(3) (a) Youngblood, W. J.; Lee, S.-H. A.; Kobayashi, Y.; Hernandez-Pagan, E. A.; Hoertz, P. G.; Moore, T. A.; Moore, A. L.; Gust, D.; Mallouk, T. E. *J. Am. Chem. Soc.* **2009**, *131*, 926. (b) Brimblecombe, R.; Koo, A.; Dismukes, G. C.; Swiegers, G. F.; Spiccia, L. *J. Am. Chem. Soc.* **2010**, *132*, 2892. (c) Li, L.; Duan, L.; Xu, Y.; Gorlov, M.; Hagfeldt, A.; Sun, L. *Chem. Commun.* **2010**, *46*, 7307. (d) Zhao, Y.; Swierk, J. R.; Megiatto, J. D.; Sherman, B.; Youngblood, W. J.; Qin, D.; Lentz, D. M.; Moore, A. L.; Moore, T. A.; Gust, D.; Mallouk, T. E. *Proc. Natl. Acad. Sci.* **2012**, DOI:10.1073/pnas.1118339109. (e) Moore, G. F.; Blakemore, J. D.; Milot, R. L.; Hull, J. F.; Song, H..; Cai, L.; Schmuttenmaer, C. A.; Crabtree, R. H.; Brudvig. G. W. *Energy Environ. Sci.*, **2011**, *4*, 2389. (f) Song, W.; Glasson, C. R. K.; Luo, H.; Hanson, K.; Brennaman, M. K.; Concepcion, J. J.; Meyer, T. J. *J. Phys. Chem. C* **2011**, *115*, 7081. (g) Song, W.; Glasson, C. R. K.; Luo, H.; Hanson, K.; Brennaman, M. K.; Concepcion, J. J.; Meyer, T. J. *J. Phys. Chem. Lett.* **2011**, *2*, 1808. (h) Li, G.; Sproviero, E. M.; McNamara, W. R.; Snoeberger, R. C.; Crabtree, R. H.; Brudvig, G. W.; Batista, V. S. *J. Phys. Chem. B* **2010**, *114*, 14214.

(4) (a) Geletii, Y. V.; Botar, B.; Kögerler, P.; Hillesheim, D. A.; Musaev, D. G.; Hill, C. L. *Angew. Chem., Int. Ed.* **2008**, 47, 3896. (b) Sartorel, A.; Carraro, M.; Scorrano, G.; Zorzi, R. D.; Geremia, S.; McDaniel, N. D.; Bernhard, S.; Bonchio, M. J. *Am. Chem. Soc.* **2008**, 130, 5006. (c) Geletii, Y. V.; Besson, C.; Hou, Y.; Yin, Q.; Musaev, D. G.; Quinonero, D.; Cao, R.; Hardcastle, K. I.; Proust, A.; Kögerler, P.; Hill, C. L. *J. Am. Chem. Soc.* **2009**, *131*, 17360. (d) Kuznetsov, A. E.; Geletii, Y. V.; Hill, C. L.; Morokuma, K.; Musaev, D. G. *J. Am. Chem. Soc.* **2009**, *131*, 6844. (e) Sartorel, A.; Miro, P.; Salvadori, E.; Romain, S.; Carraro, M.; Scorrano, G.; Valentin, M. D.; Llobet, A.; Bo, C.; Bonchio, M. *J. Am. Chem. Soc.* **2009**, *131*, 16051. (f) Besson, C.; Huang, Z.; Geletii, Y. V.; Lense, S.; Hardcastle, K. I.; Musaev, D. G.; Lian, T.; Proust, A.; Hill, C. L. *Chem. Commun.* **2010**, 46, 2784. (g) Yin, Q.; Tan, J. M.; Besson, C.; Geletii, Y. V.; Musaev, D. G.; Kuznetsov, A. E.; Luo, Z.; Hardcastle, K. I.; Hill, C. L. *Science* **2010**, *328*, 342. (h) Cao, R.; Ma, H.; Geletii, Y. V.; Hardcastle, K. I.; Hill, C. L. *Inorg. Chem.* **2009**, *48*, 5596.

(5) (a) Geletii, Y. V.; Huang, Z.; Hou, Y.; Musaev, D. G.; Lian, T.; Hill, C. L. *J. Am. Chem. Soc.* **2009**, *131*, 7522. (b) Puntoriero, F.; Ganga,G. L.; Sartorel, A.; Carraro, M.; Scorrano, G.; Bonchio, M.; Campagna, S. *Chem. Commun.* **2010**, *46*, 4725. (c) Huang, Z.; Luo, Z.; Geletii, Y. V.; Vickers, J. W.; Yin, Q.; Wu, D.; Hou, Y.; Ding, Y. Song, J.; Musaev, D. G.; Hill, C. L.; Lian, T. *J. Am. Chem. Soc.* **2011**, *133*, 2068.

(6) (a) Orlandi, M.; Argazzi, R.; Sartorel, A.; Carraro, M.; Scorrano, G.; Bonchio, M.; Scandola, F. *Chem. Commun.* **2010**, *46*, 3152. (b) Huang, Z.; Geletii, Y. V.; Musaev, D. G.; Hill, C. L.; Lian, T. *Ind. Eng. Chem. Res.* **2012**, DOI: 10.1021/ie202950h.

(7) Ghosh, P. K.; Brunschwig, B. S.; Chou, M.; Creutz, C.; Sutin, N. *J. Am. Chem. Soc.* **1984**, *106*, 4772.

(8) (a) Nutz, T.; zum Felde, U.; Haase, M. *J. Chem. Phys.* **1999**, *110*, 12142. (b) Zaban, A.; Ferrere, S.; Sprague, J.; Gregg, B. A. *J. Phys. Chem. B* **1997**, *101*, 55. (c) Anderson, N. A.; Ai, X.; Chen, D. T.; Mohler, D. L.; Lian, T. *J. Phys. Chem. B* **2003**, *107*, 14231. (d) She, C. X.; Guo, J. C.; Irle, S.; Morokuma, K.; Mohler, D. L.; Zabri, H.; Odobel, F.; Youm, K. T.; Liu, F.; Hupp, J. T.; Lian, T. *J. Phys. Chem. A* **2007**, *111*, 6832. (e) Tachibana, Y.; Moser, J. E.; Grätzel, M.; Klug, D. R.; Durrant, J. R. J. Phys. Chem. 1996, 100, 20056-20062.

(9) (a) Montalti, M.; Wahdwa, S.; Kim, W. Y.; Kipp, R. A.; Schmehl, R. H. *Inorg. Chem.* **2000**, *39*, 76. (b) Gillaizea-Gauthier, I.; Odobel, F.; Alebbi, M.; Argazzi, R.; Costa, E.; Bignozzi, C. A.; Qu, P.; Meyer, G. J. *Inorg. Chem.* **2001**, *40*, 6073.

(10) (a) Sawada, K.; Sohara, T. *J. Chem. Soc. Faraday Trans.* **1995**, *91*, 643. (b) Borman, C. J.; Custelcean, R.; Hay, B. P.; Bill, N. L.; Sessler, J. L.; Moyer, B. A. *Chem. Commun*. **2011**, *47*, 7611.

(11) Finke, R. G.; Droege, M.; Hutchinson, J. R.; Gansow, O. *J. Am. Chem. Soc.* **1981**, *103*, 1587.

(12) Brennaman, M. K.; Patroncinio, A. O. T.; Song, W.; Jurss, J. W.; Concepcion, J. J.; Hoertz, P. G.; Traub, M. C.; Iha, N. Y. M.; Meyer, T. J. *Chem. Sus. Chem.* **2011**, *4*, 216.

(13) Ardizzone, S.; Trasatti, S. *Adv. Colloid Interface Sci.* **1996**, *64*, 173.

(14) Selected examples: (a) Asbury, J. B.; Ellingson, R. J.; Ghosh, H. N.; Ferrere, S.; Nozik, A. J.; Lian, T. *J. Phys. Chem. B* **1999**, *103*, 3110. (b) Asbury, J. B.; Wang, Y. Q.; Lian, T. *J. Phys. Chem. B* **1999**, *103*, 6643. (c) Heimer, T. A.; Heilweil, E. J. *J. Phys. Chem. B* **1997**, *101*, 10990. (d) Trachibana, Y.; Haque, S. A.; Mercer, I. P.; Durrant, J. R.; Klug, D. R. *J. Phys. Chem. B* **2000**, *104*, 1198. (e) Snoeberger, R.C.; Young, K.J.; Tang, J.; Allen, L.J.; Crabtree, R.H.; Brudvig, G.W.; Coppens, P.; Batista, V.S.; Benedict, J.B. *J. Am. Chem. Soc.* **2012**, *134*, 8911. (f) Huang, J.; Stockwell, D.; Boulesbaa, A.; Guo, J.; Lian. T. *J. Phys. Chem. C* **2008**, *112*, 5203-5212. (g) Stockwell, D.; Yang, Y.; Huang, J.; Anfuso, C.; Huang, Z.; Lian T. *J. Phys. Chem. C* **2010**, *114*, 6560–6566. (h) Hanson, K.; Brennaman, M. K.; Ito, A.; Luo, H.; Song, W.; Parker, K. A.; Ghosh, R.; Norris, M. R.; Glasson, C. R. K.; Concepcion, J. J.; Lopez, R.; Meyer, T. J. *J. Phys. Chem. C* **2012**, *116*, 14837.

(15) Huang, Z.; Hill, C. L.; Lian, T. unpublished results.

(16) (a) Asbury, J. B.; Anderson, N. A.; Hao, E.; Ai, X.; Lian, T. *J. Phys. Chem. B.* **2003**, *107*, 7376. (b) Anderson, N. A.; Lian, T. *Ann. Rev. Phys. Chem.* **2005**, *56*, 491. (c) Benko, G.; Myllyperkio, P.; Pan, J.; Yartsev, A.P.; Sundstrom, V. *J. Am. Chem. Soc* **2003**, *125*, 1118.

(17) (a) Ai, X.; Anderson, N. A.; Guo, J. C.; Lian, T. *J. Phys. Chem. B* **2005**, *109*, 7088. (b) Asbury, J. B.; Hao, E.; Wang, Y. Q.; Ghosh, H. N.; Lian, T. *J. Phys. Chem. B* **2001**, *105*, 4545.

(18) (a) Hagfeldt, A.; Gratzel, M. *Chem. Rev.* **1995**, *95*, 49. (b) Enright, B.; Fitzmaurice, D. *J. Phys. Chem.* **1996**, *100*, 1027.

(19) Green, A. N. M.; Palomares, E.; Haque, S. A.; Kroon, J. M.; Durrant, J. R. *J. Phys. Chem. B* **2005**, *109*, 12525.

(20) Natali, M.; Orlandi, M.; Berardi, S.; Campagna, S.; Bonchio, M.; Sartorel, A.; Scandola, F. *Inorg. Chem.* **2012**, *51*, 7324.

(21) Pelet, S.; Moser, J.-E.; Grätzel, M. *J. Phys. Chem. B* **2000**, *104*, 1791.

(22) (a) Ardo, S.; Sun. Y.; Staniszewski, A.; Castellano, F. N.; Meyer, G. J. *J. Am. Chem. Soc.* **2010**, *132*, 6696. (b) Ardo, S.; Sun, Y.; Castellano, F. N.; Meyer, G. J. *J. Phys. Chem. B* **2010**, *114*, 14596.

(23) (a) Hanson, K.; Brennaman, M. K.; Luo, H.; Glasson, C. R. K.; Concepcion, J. J.; Song, W. ; Meyer, T. J. *ACS Appl. Mater. Interfaces* **2012**, *4*, 1462.

Authors are required to submit a graphic entry for the Table of Contents (TOC) that, in conjunction with the manuscript title, should give the reader a representative idea of one of the following: A key structure, reaction, equation, concept, or theorem, etc., that is discussed in the manuscript. Consult the journal's Instructions for Authors for TOC graphic specifications.